Analysis of the AC Electrical Response for (Ba,Pb)TiO_3 Positive Temperature Coefficient Ceramics

Chun-Hung Lai and Tseung-Yuen Tseng

Abstract— **AC electrical properties of positive temperature coefficient of resistance (PTCR) ceramics of composition $Ba_{0.347}Pb_{0.65}La_{0.003}Ca_{0.005}Ti_{0.995}O_3$ with Curie point Tc $\approx$ 380°C were studied. A combined imaginary impedance/modulus plot was adopted to identify the appropriate equivalent circuit. Analysis of such circuit modified with a frequency dependent capacitor C_n gives satisfactory interpretation of the commonly observed inclined semicircle in the complex impedance plane. The exponent n, which is extracted from the depression angle and suggested to be associated with the "loss" degree of the material, shows a temperature dependence similar to that of a useful parameter extracted from the ac conductivity–frequency measurements. Both are ascribed to the conduction characteristics of the grain boundary, whose resistivity anomaly is the main contribution to PTCR jump. The validity of the present methodology is assessed not only by fitting well the observed non-ideality of real ac response, but also by confirming the Curie–Weiss behavior of the calculated grain boundary capacitance, which is the essence of well-accepted barrier theory (Heywang–Jonker model) proposed to explain the PTCR effect.**

I. Introduction

THE electrical resistance of n-doped polycrystalline barium titanate ceramics increases several orders of magnitude near the ferroelectric transition temperature T_c, known as the positive temperature coefficient of resistance (PTCR) effect [1]. PTCR materials with higher onset temperatures, achieved by compositional modification of Pb^{2+} for Ba^{2+}, can find applications in heating elements. However, the difficulty of manufacture increases due to the loss of Pb during the sintering process and the poor sinterability of (Ba,Pb)TiO_3 powder compacts, especially for those using commercial $BaTiO_3$ powder as a raw material. Until now the investigations of PTCR behavior were rarely conducted on samples with T_c up to 350°C [2]–[4].

It is believed that the PTCR phenomenon is a grain boundary resistive effect [5]–[7]. Based on the presence of surface acceptor states at the grain boundary, and treatment of the potential in the depletion region as a Schottky type, Heywang's barrier model is the most widely accepted to explain the electrical structure of the grain boundary [6]. Later, Jonker extended this model by considering the spontaneous polarization effect below T_c to explain the simultaneous low resistance and low permittivity before the anomalous jump [7]. From the previous works that confirmed the validity of Heywang-Jonker model for the interpretation of PTCR phenomenon, we perceive the variation of the depletion width near the grain boundary as a function of temperature [8], [9]. With the approximately constant value within $T_c \sim T_{max}$ as a reference, the depletion width is decreased below T_c, as well as above T_{max}, where T_{max} is the temperature corresponding to the maximum in resistivity. The former is caused by the compensation of acceptor charges by the ferroelectric polarization, while the latter is due to depopulation of occupied states at higher temperatures [9].

In addition to direct examination of grain and/or grain boundary [10], complex impedance or admittance method of characterizing the electrical properties of polycrystalline materials is commonly adopted to separate and identify the inter/intra granular impedances [5], [11]–[13]. Typically, results from impedance spectroscopy measurements are analyzed via Nyquist plots, in which the imaginary part is plotted against the real part. The resulting curve is parameterized by the applied frequency, with low frequencies at a high real-axis intercept and high frequencies at a low one. Depending on the distinctive orders of magnitude for the relaxation time, which is defined as the time constant RC in the equivalent circuit to be an indication of the transport process [11]–[14], a series array of parallel RC elements may give rise to independent or overlapping semicircular arcs in the two complex planes. Complex impedance measurements are of great interest because they allow separation of the contributions of the grains and grain boundaries to the total impedance. Maiti and Basu applied this concept for the first time to analyze the $BaTiO_3$-based PTC thermistor [11]. They investigated the effect of electrode materials on the real axis intercepts of the low frequency arcs at room temperature and concluded that the interface resistance of In-Ga electrode was negligible, while the high frequency arcs were used to determine the inter/intra resistances. Tseng and Wang then conducted a series of complex impedance plots under different temperatures and verified that the PTC resistivity jump was a grain boundary phenomenon [5]–[7].

The shape of real Nyquist plot is usually analyzed using equivalent circuit analysis, where a collection of resistors and capacitors arranged in various combinations of series and parallel circuits are used to duplicate the experimental spectrum. The combination of parallel RC components in a series can easily reveal, along the conduction path, different types of

Manuscript received August 20, 1993. This work was supported in part by the National Science Council of the Republic of China under Project NSC 81-0404-E009-103.

The authors are with the Department of Electronics Engineering and Institute of Electronics, National Chiao-Tung University, Hsinchu, Taiwan, Republic of China.

IEEE Log Number 9401774.

structures, e.g., insulating grain boundary layers and semiconducting grains. Theoretically speaking, one may construct the "exact" equivalent circuit, based on reasonable physical justifications, with each element corresponding to any specific conduction mechanism, although this qualitative description often lacks experimental evidence in view of the comparison between the real and the ideal (theoretical) electrical response. Obviously, there exists two significant drawbacks to equivalent circuit analysis: (1) different equivalent circuits can produce the same electrical response, making the microstructure/circuit element relationships difficult to establish, and (2) once the equivalent circuit becomes more complicated than simple combinations of two or three elements, intuitive understanding of the material's response may be lost. Actually, the real ac electrical response always indicates some deviations from the theoretical predictions. Specifically, by analogy with the well-known Cole–Cole construction in the complex permittivity plane [15], the complex impedance loci of the experimental data are approximated by an inclined semicircle [16]. Some modified empirical expressions have been proposed to describe the appearance of departure, in varying degrees, from the Debye response. And the qualitative "interpretation" in terms of the so-called distributions of relaxation times has always been employed by using the depression angle to provide a "measure" of the breadth of this distribution [17]. Nevertheless, any physical significance of these tilting operations has yet to be established [15].

Alternatively, Jonscher pointed out the phenomena of "non-Debye" response of solid dielectrics, and Yeh and Tseng proved it quantitatively useful by introducing this universal frequency-dependent capacitance concept [18]–[20]. In this study, we try to develop as simple a methodology as possible for the analysis of the "depressed" circular arcs in impedance diagrams, which are exhibited by most PTCR samples, while still incorporating the important features of the conduction process so that the results would be meaningful. With the use of a simple circuit modified by a frequency-dependent capacitor to model the PTCR ceramics, a procedure to extract those component values is established, and useful physical information can be obtained from the temperature dependence of the individual circuit parameters. Interpretation of ac electrical data is then given intuitively in terms of the parameters calculated.

II. Theory

A. Parameter Relation

The electrical parameters used to characterize the ac response of the sample are impedance Z^*, admittance Y^*, and modulus M^*. They have the following transformation relationship:

$$Z^* = R - jX = (Y^*)^{-1} = (G + jB)^{-1} \tag{1}$$

$$M^* = j\omega C_0 Z^* \tag{2}$$

where R, X, G, B are symbols of resistance, reactance, conductance and susceptance, respectively, and all are presented in units of Ω or S. C_0 is obtained from multiplying the free space permittivity ϵ_0 by A/t, where A is the cross-sectional area of the sample and t the thickness. Resistivity or conductivity can be obtained by considering the geometrical factor A/t. Sample in this study has $A/t \approx 4.2$ cm. And ω is the angular frequency in unit of radians per second.

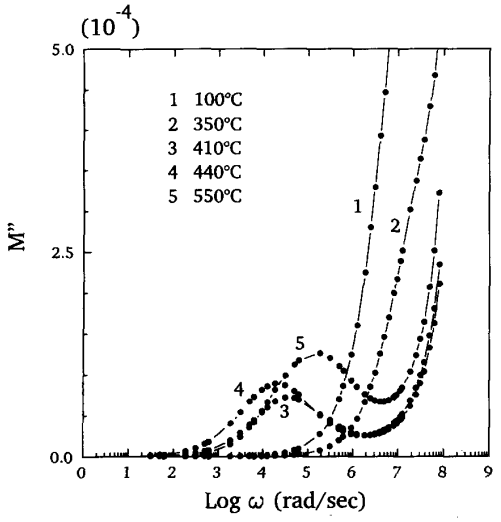

Fig. 1. Modulus M'' spectroscopic plot against frequency. M'' peak as a function of temperature (above T_c) is depicted in Fig. 9.

Obviously, one can get $RG \neq 1$ from (1). With the loss tangent D defined as $G/|B|(= R/|X|)$, it can be derived easily from (1) to have the relation: $RG = D^2/(1 + D^2)$. The relation $R \approx 1/G$ is valid when $D \gg 1$. The frequency-dependent nature for D causes the discrepancy in the variations of R and G with frequency. In other words, one can infer the R's frequency dependence from G's only when D shows a plateau within a certain frequency range.

B. Equivalent Circuit Determination

To extract information from experimental ac data, an equivalent circuit is needed to provide a realistic representation of the electrical properties. From ac circuit theory, one should note that it is usually possible to find more than one equivalent circuit that fits a given data set. A combined plot of the impedance/modulus spectroscopic analysis was found to be invaluable as a first step to identify the appropriate circuit [21], [22]. In the light of performance for a single parallel RC element, which is commonly used to represent one kind of structure or interface in the sample, it can be shown that the peak is proportional to $1/C$ and R for M'' and X plots, respectively, and both occur at frequency $\omega_{\max} = 1/RC$. Peaks for a series circuit are expected to be distinct only if the time constants RC differ by at least two orders of magnitude. Figs. 1 and 2 show plots of the measured imaginary component (M'', $\log X$ vs $\log \omega$). Linear plots for M'' are shown to display the $1/C$ linear relationship with temperature (see later in Fig. 9), while the log scales are used for X due to the orders of magnitude.

Evidently, by comparison of Fig. 1 with Fig. 2, one single RC component seems to sufficiently characterize the dominant

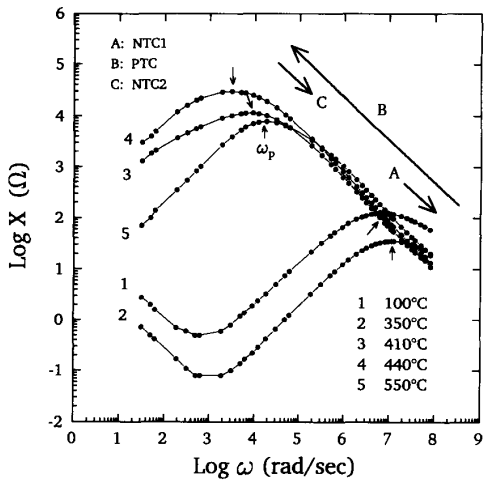

Fig. 2. Impedance spectra of the sample at different temperatures. The arrows indicate the R'_{gb} variation as temperature increases along the distinctive regions of resistivity-temperature curve, which labeled as NTC1, PTC and NTC2. Peak position is denoted to stress its dependence on R_{gb}.

response of the present sample. Several points should be clarified before we proceed. First, an impedance element representing the ceramic-electrode interface has been ignored in cases where the contact resistance is small, as with the present In/Ga electrode, although apparently the contact capacitance (considerably large compared with grain boundary capacitance C_{gb} and grain capacitance C_g) causes an additional low frequency effect in X at $T < T_c$. However, we simplify the methodology by ignoring this contribution from electrode effect. This assumption is justifiable by the observation that the electrode effect is manifested only at low frequencies, resulting in the situation that the contact capacitance cannot be extracted quantitatively from the experimentally-observed single circular arc, which is ascribed to the contribution from grain boundary. Secondly, for the reason that $R_{gb} \gg R_g$ (the grain boundary resistance is much higher than that of grain for PTCR sample) and $C_{gb} \gg C_g$ (due to the larger grain size compared to the depletion width and the semiconductor character of the grain), the peak in M'' and X plot is ascribed to the grain boundary's contribution. The peak associated with grain is outside the measuring frequency range. Thirdly, the slight overlap of $R_{gb}C_{gb}$ and R_gC_g accounts for the noncoincidence of the observed M'' and X peaks on frequency scale (M'' slightly higher due to high $1/C_g$ value). The overlapping RC elements exert less uncertainty in interpretation of X plots due to the large difference between R_g and R_{gb}, thus the correctness of calculated grain boundary capacitance data from X is raised. Finally, one can infer that C_{gb} is decreasing above T_c from M'' plot, assuming the contribution from $1/C_g$ as a constant background. We will discuss this behavior thoroughly as well as the comments on X plot later.

With the finite grain resistance R_g taken into consideration, a simple circuit shown in Fig. 3 is adopted as the electrical equivalent representation for the present sample. If the true behavior of a more complicated circuit is to be properly recognized, a very wide testing frequency range is needed.

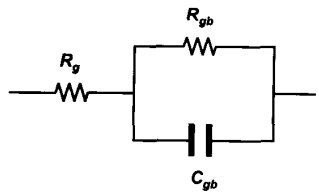

Fig. 3. Conventional equivalent circuit model for PTCR ceramics.

C. Parameter Extraction

Our main objective in this study is to investigate the distorted shape of the complex plot and to gain an understanding of the physical phenomena occurring in the material. By using the simple circuit in Fig. 3 as a framework, a frequency independent capacitor is modified to achieve this goal. The dispersive frequency-dependent capacitance, which Jonscher terms as "non-Debye" (or "universal") capacitance, is given by [18]

$$C_n(\omega) = C(j\omega)^{n-1} \tag{3}$$

in which the exponent n defines the frequency dependence and C is a constant. A parallel combination of this capacitance and a frequency-independent resistance will give an inclined circular arc in the complex impedance plane [13]. Using the circuit model as shown in Fig. 3 and letting the grain boundary capacitance be $C_{gb}(j\omega)^{n-1}$, then the full expression of the impedance can be written as follows:

$$Z(\omega) = R_g + \frac{1}{\frac{1}{R_{gb}} + C_{gb}(j\omega)^n}. \tag{4}$$

To demonstrate the effect of n on the shape of the circular arc in logarithmic coordinates, which are necessitated by the orders of magnitude exhibited in the resistivity anomaly of PTCR ceramics, Fig. 4 gives the schematic presentation with different values of n as indicated, while the inset shows the linear scale presentation for comparison. A straight line of slope, 1/2 with the left part becoming a vertical line at appropriate abscissa in the log-log scales represents the part of semicircle ($n = 1$) in linear plot next to the origin. The dotted line $R = X$ represents a reference—above it ($n > 1/2$) the loss component is less than the capacitive component, while the reverse ($n < 1/2$) is true below this line. One should note that the nearly constant R may not be observed experimentally due to limited frequency range of the measuring apparatus, as with the present case. Another reason is in the non-ideal character of the sample, i.e., $n \neq 1$.

It is obvious that a larger depression angle θ will reflect a smaller n, corresponding to the nature of a more lossy material. Let $\phi = (\pi/2)n$ and after some manipulations with $R_{gb} \gg R_g$ assumed, one can easily derive from (4) that the peak position

$$(R_p, X_p) = \left(\frac{R_{gb}}{2}, \frac{R_{gb}}{2}\tan(\phi/2)\right)$$

and occurs at frequency:

$$\omega_p^n = (R_{gb}C_{gb})^{-1} \tag{5}$$

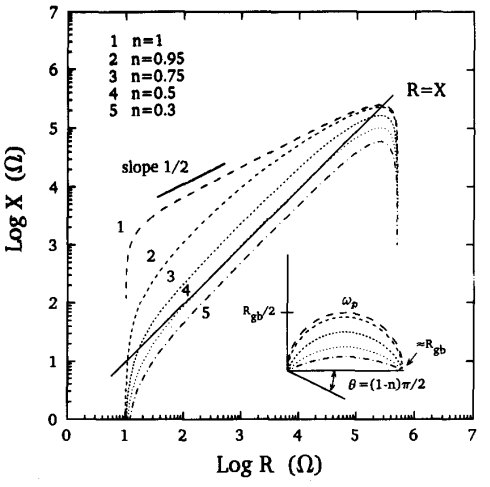

Fig. 4. Schematic log–log representation of depressed complex impedance planes, with the exponent n corresponding to the depression angle. The inset shows the linear scale one for comparison.

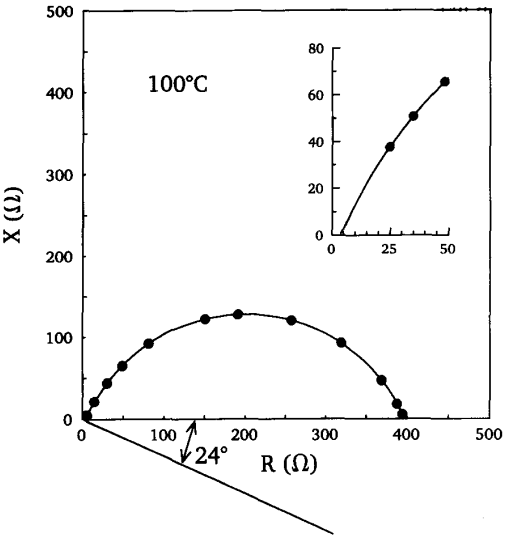

Fig. 5. Typical Nyquist plot in linear scales at 100° C and inset is the corresponding expanded section near the origin, from which one can easily determine the n and R_g.

with the depression angle $\theta = \pi/2 - \phi$. Therefore, we can easily construct the algorithm to extract the various element values. The resistance values are derivable from the circular arc intercepted on the R-axis; and the capacitance values C_{gb} can be derived from the expression for measured ω_p in (5), where n is determined experimentally from the depression angle θ. Here care should be taken of the Rg value extraction, whose value is obtained from the least square fit, especially for $T > T_c$ where $R_{gb} \gg R_g$. Fig. 5 shows the typical linear-scale Nyquist plot and one can easily see the determination of θ and R_g.

III. Experimental

A. Sample Preparation

The raw materials in preparing the specimen were commercially available powders of $BaTiO_3$, PbO, La_2O_3, TiO_2 and $CaCO_3$. Powders with formulation of $Ba_{0.347}Pb_{0.65}La_{0.003}-Ca_{0.005}Ti_{0.995}O_3$ were mixed and ball-milled with deionized water in a plastic jar for 24 h. Then the milled slurry was dried by an IR lamp to evaporate the water, and calcined at 950° C for 90 min in an Al_2O_3 crucible. The obtained semiconducting powder was pressed into disks with nominal dimensions of 1 cm in diameter by 0.2 cm thick under a pressure of 900 psi. The pellet weight was about 0.6 g. These respective compacts, covered by the same sample powders with a weight ratio of approximately 3:2 to the pellets were then stacked inside a crucible with lids tightly fitted and fired at 1200° C for 30 min. Heating and cooling rates were kept at 25°C/min and 600°C/h, respectively. The average weight loss of the sample after sintering did not exceed 1 wt%. Fig. 6 is a scanning electron micrograph of fracture surfaces for the present sample. The average grain size determined by the linear intercept methods and the fired bulk density obtained by Archimedes' techniques, are 2.4 μ m and 6.6 g/cm^3, respectively. The specimen containing lead content

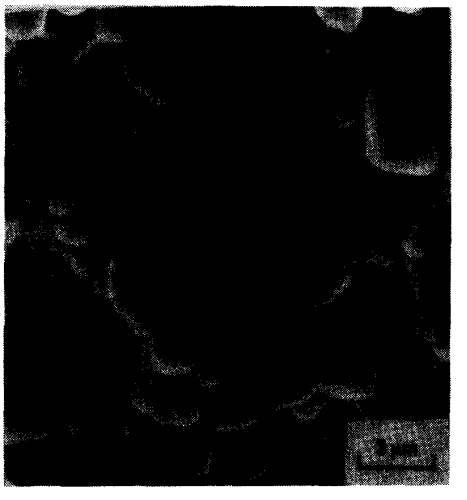

Fig. 6. Scanning electron micrograph of fracture surface of samples in the present study.

65 at% used in this study is really representative of high-T_c PTCR ceramics [5]. Therefore, the ac electrical response, and, hereafter, the developed methodology and conclusion, allow one to scan the properties of semiconducting (Ba,Pb)TiO_3 ceramics.

B. Electrical Measurement

The electrical properties were measured by using a two-probe method from 50°C to 600° C in air by HP4140B (pA meter/dc voltage source) and HP4192A (LF impedance analyzer) at zero bias with ac signals amplitude of 1 V. Data were taken at frequencies ranging from 13 MHz to 5 Hz, and corrected for lead inductance and stray residuals. Rubbed

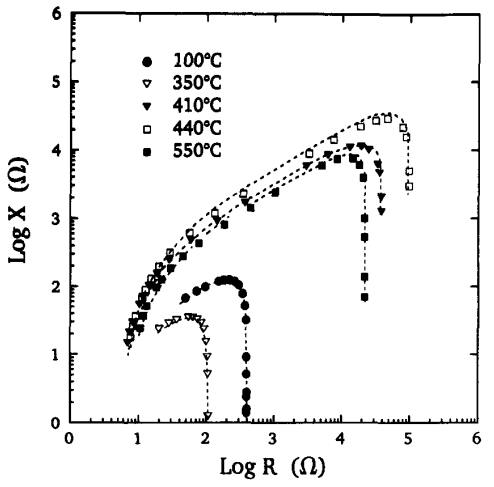

Fig. 7. The measured (symbols) and calculated (dotted lines) complex impedance curves in full logarithmic coordinates at different temperatures.

TABLE I
MEASURED AND CALCULATED PARAMETRIC VALUES AT PARTICULAR CHOICE OF TEMPERATURES, RESIDING IN DIFFERENT POSITIONS OF THE RESISTIVITY–TEMPERATURE CURVE. THE SLOPE m OBTAINED FROM FIG. 10 IS ALSO LISTED.

	100°C	350°C	410°	440°C	550°C
R_g (Ω)	3.6	4.8	6	7	8
R_{gb} (Ω)	395	105	38 800	96 000	23 500
ω_p (rad/s)	8M	13 M	10 k	4.2 k	33 k
n	0.73	0.72	0.938	0.96	0.932
C_{gb} (nF)	23	72	4.56	3.46	2.62
m	0.34	0.31	1.33	1.394	1.32

with In-Ga alloy (40:60) to ensure the ohmic contact at the ceramic-metal interface, the electrode surfaces of the pellet were also covered with thin steel sheets pressed on to prevent the electrode material from vaporizing during heating. Heated at a rate of 3°C/min in a programmable furnace, samples were held at the desired temperature for enough time to equilibrate with the temperature readings before each testing was made. Data obtained in this way are reversible after experiencing such thermal cycles.

IV. RESULTS AND DISCUSSION

Based on the concept and procedure described in the Theory section to extract various parameters, the resultant diagram containing the measured (symbols) and the calculated (dotted lines) impedance plot is shown in Fig. 7, at particular choice of temperatures below and above the Curie point $T_c \approx 380$°C. The relevant parametric values are listed in Table I.

Obviously, the non-Debye behavior at all temperatures can be well simulated just by adjusting the circuit model in Fig. 3 with the operation of a "non-Debye" capacitance substitution. Also, from Table I, the following conclusions with regard to the PTCR characteristics can be drawn:

1) R_g:

The resistance of grains R_g increases slightly with temperatures, which may be the consequence of the declining mobility for charge carriers [23].

2) R_{gb}:

The resistivity anomaly displayed by R_{gb} implies that the PTCR effect is a grain boundary phenomenon even below the Curie point [5], [7], [9].

3) ω_p:

The frequency where the peak occurs (ω_p) is inverse proportional to $R_{\rm gb}$. With reference to (5), and neglecting the effects of n and $C_{\rm gb}$ for the moment, the variations of ω_p observed are understandable. With this dependence of ω_p and $X_{\rm p}$ on $R_{\rm gb}$, the reason for the transition of curve shape in Fig. 2 is evident by considering $R_{\rm gb}$'s variation with temperature.

The three distinctive segments on the resistivity–temperature curve, which are divided by $T_{\rm min}$ and $T_{\rm max}$ as NTC1-PTC-NTC2 (see Fig. 11 also), are denoted by the arrows in Fig. 2 for clarity and intended to be an indication of the $R_{\rm gb}$'s changes. $T_{\rm min}$ and $T_{\rm max}$ are temperatures corresponding to the minimum and maximum in resistivity, 370°C and 440°C, respectively.

4) n:

In contrast with ω_p, n is proportional to R_{gb} as a function of temperature. Jonscher showed that the exponent n is related to the extent of the screening effect caused by the hopping charges or dipoles when they cannot follow the changes of polarization brought about by an alternating electric field [18]. This is consistent with the interpretation of a smaller n for a lossy material, corresponding to a small $R_{\rm gb}$. Accordingly, one may infer that the loss factor $D(= G/|B|)$ in the low resistance state below T_c is higher than that above T_c. The relation of loss factor vs temperature measured at 10 kHz clarifies this point, as shown in Fig. 8. The seemingly "complementary" behavior against temperature between D and R_{gb} can thus be interpreted well in terms of the parameter n's physical significance. This point of view is supported by the G vs ω measurement, as will be discussed later.

5) $C_{\rm gb}$:

$C_{\rm gb}$ is proportional to $\epsilon_{\rm r}/b$, where $\epsilon_{\rm r}$ is the dielectric constant and b the width in the depletion region in one grain. In view of the temperature dependent constants $\epsilon_{\rm r}$ and b, three distinctive characteristics revealed by data can be explained without difficulty, including: (i) the larger $C_{\rm gb}$ below T_c than above T_c; (ii) the rising $C_{\rm gb}$ below $T_{\rm c}$; (iii) the decreasing $C_{\rm gb}$ above T_c.

The features dominated by $\epsilon_{\rm r}$ account for (ii) and (iii), i.e., an approximately symmetric $\epsilon_{\rm r} - T$ curve with a peak at T_c (increasing below T_c and decreasing above T_c as temperature increases). Specifically, above T_c, the Curie–Weiss law states that $1/\epsilon_{\rm r}$ increases with temperature for ferroelectric materials. Fig. 9 shows the results of $1/C_{\rm gb}$ vs temperature, in which a straight line plus a second region with smaller slope is observed. M'' plot, where the peak is proportional to $1/C_{\rm gb}$ by neglecting the contribution from grain, is also shown for comparison.

The first linear segment lies in the temperature region of 410° C$\sim$ 440° C, falling within $T_{\rm c} \sim T_{\rm max}$ where a constant

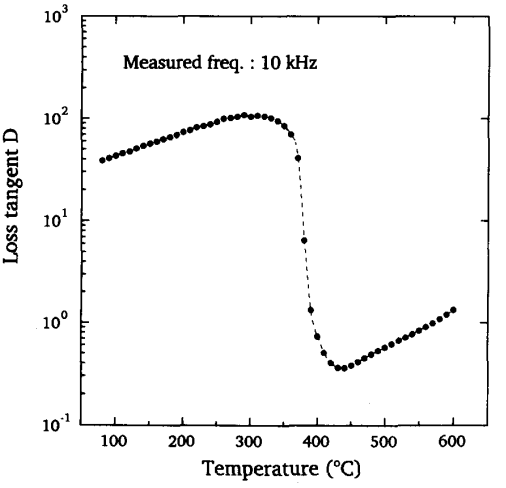

Fig. 8. Typical curve of loss tangent D versus temperature, measured at 10 kHz.

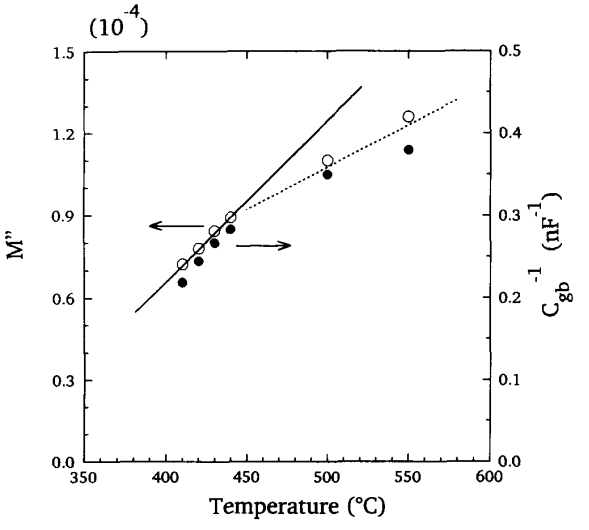

Fig. 9. Construction of $1/C_{gb}$ and M'' versus temperature to illustrate the validity of Curie–Weiss law above T_c.

occupied acceptor-states density, and therefore a constant b, is assumed [8] and theoretically confirmed [9]. Due to $1/C_{\rm gb} \propto 1/\epsilon_r$, the linearity of $1/C_{\rm gb}$ versus T as shown can be thought of as a direct proof of the Curie–Weiss law. Here we should note that the noncoincidence of Curie point $T_{\rm c}$ and Curie temperature T_0: the former is the actual temperature of inversion of the structure while the latter is a formula constant obtained by extrapolation. They generally do not coincide [24]. At higher temperatures above $T_{\rm max}$, the gradual depopulation of the surface traps reflects itself a smaller b, and the resulting discrepancy occurs. The quantitative interpretation of this phenomena has been given in a previous paper [9].

With regard to (i), the reduced trap density caused by polarization compensation below T_c is responsible. As briefly stated in the Introduction, the depletion region near the grain boundary is narrowed because the acceptor states are partly

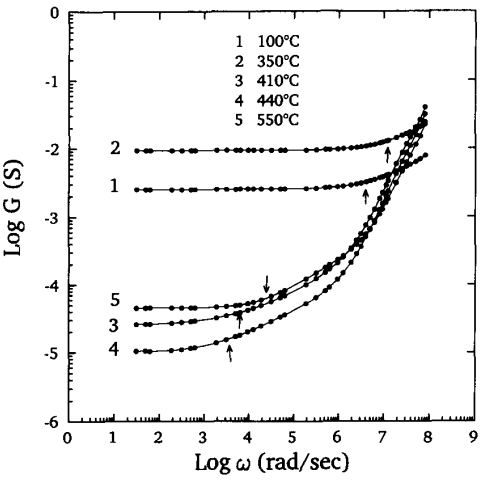

Fig. 10. Conductance behavior of the sample at different temperatures.

compensated by the discontinuous values of normal spontaneous polarizations. The effect of a small b as a result of the ferroelectric properties prevailing below Curie point accounts for the larger $C_{\rm gb}$ below $T_{\rm c}$ than those above $T_{\rm c}$ [7], [9].

It is sometimes useful to analyze ac data using the admittance formalism either as the complex plane or as spectroscopic plots. The variation with frequency of conductance G at different temperatures is plotted in Fig. 10, where all curves seem to obey the power-law frequency dependence given by

$$G(\omega) = G_0(T) + a(T)\omega^{m(T)}. \tag{6}$$

This implies [14] that the hopping mechanism for carrier conduction, known as polaron [23], can also occur in the $BaTiO_3$-based PTCR.

The conductance plateau $G_0(T)$ at low frequency, which is believed to be due to the dc conduction of the material, displays the orders of magnitude of $R_{\rm gb}^{-1}$. A high frequency plateau corresponding to R_g is not observable within the accessible frequency range, as can be seen from the still decreasing R in Fig. 7. High frequency dispersion in G commences approximately near $\omega_{\rm p}$, and its temperature dependence is expected to be inverse proportional to $R_{\rm gb}$'s. Fig. 11 demonstrates the characteristics of $1/G$ versus temperature construction, in which we want to elucidate the more strongly frequency-dependent nature of a high resistance state (a lower ω_p). Note that $1/G$ is manipulated by A/t to get the equivalent parallel resistivity $\rho_{1/G}$, and the dc measured resistivity is also shown. As expected for the $\rho_{1/G}$ variation against temperature, the frequency effect is more obvious at higher resistance by considering the G's frequency dependence.

The values shown in Table I have been calculated with emphasis on the temperature dependence of the exponent m, which is determined from the monotonously rising region of the G-ω curve. Bai and Tseng have interpreted m to be an indication of the probability of a carrier trapped in the localized states [14]. For PTCR sample, consistent results support this interpretation that the state with lower G_0, and therefore with higher $R_{\rm gb}$, will produce a higher value for m. This is in

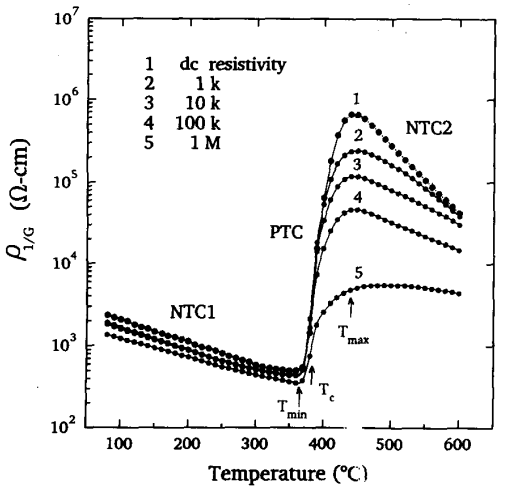

Fig. 11. Equivalent parallel resistivity against temperature under different frequencies, with the dc measured resistivity shown for comparison.

accordance with the implication of a larger n for a more insulated grain boundary, as investigated previously for the larger R_{gb}.

V. Conclusions

The ac electrical response for (Ba,Pb)TiO_3 PTCR ceramics can be explained satisfactorily based on an equivalent circuit with a frequency dependent capacitor substitution. The physical significance of parameter n, which exhibits itself in the depression angle of the conventionally observed depressed circular arcs, is interpreted in terms of the insulating properties of material involved. By examining loss tangent (D in Fig. 8) and conductivity behavior (m in Fig. 10), agreement of the information thus obtained with that of n justifies the proposed physical meaning of this calculated parameter, which is usually ignored when constructing a complex plane for PTCR ceramics. From the comments on n in this study, one can conclude that a higher resistance state above T_c will give a more ideal semicircular than that below T_c. And the results also show that only grain boundary contributes to the PTCR effect. The validity of Curie–Weiss law is proven with the help of the calculated grain boundary capacitance, which in turn proves the correctness of the present analysis.

References

[1] P. W. Haaijman, R. W. Dam, and H. A. Klasens, "Method of preparation of semiconducting materials," Ger. Pat. No. 929350, June, 1955.
[2] M. Kuwabara, S. Suemure, and M. Kawahara, "Preparation of high-curie-point barium-lead titanate ceramics and their PTCR characteristics," *Amer. Ceram. Soc. Bull.*, vol. 6, pp. 1394, 1985.
[3] N. H. Chan and D. M. Smyth, "Defect chemistry of donor-doped $BaTiO_3$," *J. Amer. Ceram. Soc.*, vol. 67, pp. 285, 1984.
[4] C. H. Lai and T. Y. Tseng, "Preparation and ac electrical response analysis for (Ba,Pb)TiO_3," *J. Amer. Ceram. Soc.*, vol. 76, pp. 781, 1993.
[5] T. Y. Tseng and S. H. Wang, "ac electrical properties of high-curie-point barium-lead titanate PTCR ceramics," *Mat. Lett.*, vol. 9, pp. 164, 1990.
[6] W. Heywang, "Barium titanate as a semiconductor with blocking layers," *Solid-State Electron.*, vol. 3, pp. 51, 1961.
[7] C. H. Jonker, "Some aspects of semiconducting barium titanate," *Solid-State Electron.*, vol. 7, pp. 895, 1964.
[8] J. Illingsworth, H. M. Al-Allak, A. W. Brinkman and J. Woods, "The influence of mn on the grain-boundary potential barrier characteristics of donor-doped $BaTiO_3$ ceramics," *J. Appl. Phys.*, vol. 67, pp. 2088, 1990.
[9] C. H. Lai, Y. Y. Lu and T. Y. Tseng, "Calculations and modeling of grain-boundary acceptor states for (Ba,Pb)TiO_3 positive temperature coefficient ceramics," *J. Appl. Phys.*, vol. 74, no. 5, Sept. 1993.
[10] H. Nemoto and I. Oda, "Direct examination of PTC action of single grain boundaries in semiconducting $BaTiO_3$ ceramics," *J. Amer. Cer. Soc.*, vol. 63, pp. 398, 1980.
[11] H. S. Maiti and R. N. Basu, "Complex-plane impedance analysis for semiconducting barium titanate," *Mat. Res. Bull.*, vol. 21, pp. 1107, 1986.
[12] I. M. Hodge, M. D. Ingram and A. R. West, "Impedance and modulus spectroscopy of polycrystalline solid electrolytes," *J. Electroanal. Chem.*, vol. 74, pp. 125, 1976.
[13] A. K. Jonscher and J. M. Reau, "Analysis of the complex impedance data for β-PbF_2, *J. Mat. Sci.*, vol. 13, pp. 563, 1978.
[14] S. N. Bai and T. Y. Tseng, "The effect of grain boundaries on the electrical properties of zinc oxide-based varistor," *J. Electron. Mat.*, vol. 21, pp. 1073, 1992.
[15] K. S. Cole and R. H. Cole, "Dispersion and adsorption in dielectrics: I. alternating current characteristics," *J. Chem. Phys.*, vol. 9, pp. 341, 1941.
[16] A. K. Jonscher, "Analysis of the alternating current properties of ionic conductors," *J. Mat. Sci.*, vol. 13, pp. 553, 1978.
[17] J. F. Bauerle, "Study of solid electrolyte polarization by a complex admittance method," *J. Phys. Chem.*, vol. 30, pp. 2657, 1969.
[18] A. K. Jonscher, "The interpretation of non-ideal dielectric admittance and impedance diagrams," *Phys. Status Solidi A*, vol. 32, pp. 665, 1975.
[19] Y. C. Yeh and T. Y. Tseng, "Electrical properties of K_2O-doped $Ba_{0.5}Sr_{0.5}TiO_3$ ceramic humidity sensor," *IEEE Trans. Comp. Hybrids, Manuf. Technol.*, vol. CHMT-12, pp. 259, 1989.
[20] Y. C. Yeh, T. Y. Tseng and D. A. Chang, "Electrical properties of TiO_2-$K_2Ti_6O_{13}$ porous ceramic humidity sensor," *J. Amer. Ceram. Soc.*, vol. 73, pp. 1992, 1990.
[21] I. M. Hodge, M. D. Ingram and A. R. West, "A new method for analyzing the a.c. behavior of polycrystalline solid electrolytes," *Electroanal. Chem. Interfacial Electrochem.*, vol. 58, pp. 429, 1975.
[22] D. C. Sinclair and A. R. West, "Impedance and modulus spectroscopy of semiconducting $BaTiO_3$ showing positive temperature coefficient of resistance," *J. Appl. Phys.*, vol. 66, pp. 3850, 1989.
[23] H. Ihrig, "On the polaron nature of the charge transport in $BaTiO_3$," *J. Phys. C*, vol. 9, pp. 3469, 1976.
[24] B. Jaffe, W. Cook, and H. Jaffe, *Piezoelectric Ceramics*. London and New York: Academic, 1971, p. 12.

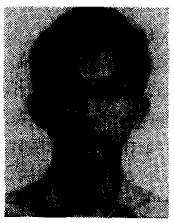

Chun-Hung Lai was born in Taichung, Taiwan, on July 16, 1966. He received the B.S. degree from the Department of Electronics Engineering, National Chiao-Tung University, Hsinchu, Taiwan, R.O.C., in 1989. Currently, he is working towards the Ph.D. degree at the Institute of Electronics at National Chiao-Tung University.

His current research interest is in the calculation and modeling of grain-boundary characteristics for ceramic materials.

Tseung-Yuen Tseng received the Ph.D. degree in electro-ceramics from the School of Materials Engineering from Purdue University, West Lafayette, IN, in 1982.

Before joining Chiao-Tung University, Hsinchu, Taiwan, R.O.C., in 1983, where he is now a Professor in the Department of Electronics Engineering and the Institute of Electronics, he was briefly associated with the University of Florida. His professional interests are electronic ceramics, ceramic sensors, and high-temperature ceramic superconductors.

Dr. Tseng is a member of the American Ceramic Society. He has authored or coauthored more than 70 technical journal papers.